Batteries & Supercaps

Research Article
doi.org/10.1002/batt.202300156

Chemistry Europe
European Chemical Societies Publishing

www.batteries-supercaps.org

Special Collection

Toward the Formation of the Solid Electrolyte Interphase on Alkaline Metal Anodes: Ab Initio Simulations**

Daniel Stottmeister*[a] and Axel Groß*[a, b]

The transition from lithium-based energy storage to post lithium systems plays a crucial part in achieving an environmentally sustainable energy infrastructure. Prime candidates for the replacement of lithium are sodium and potassium batteries. Despite being critical to battery performance, the solid electrolyte interphase (SEI) formation process for Na and K batteries remains insufficiently understood, especially compared to the well-established lithium systems. Using ab initio molecular dynamics (AIMD) simulations based on density functional theory (DFT) calculations, we study the first steps of SEI formation upon the decomposition of typical solvent molecules on lithium, sodium and potassium metal anodes. We find that two dominant products form during the early SEI formation of cyclical carbonates on alkali metal anodes, carbon monoxide and alkali-carbonate. The carbonate-producing reaction is thermodynamically favorable for all tested metals, however, Na and K exhibit a much stronger selectivity than Li towards carbonate formation. Furthermore, we propose a previously unknown reaction mechanism for the CO polymerization on metallic lithium.

Introduction

With the transition from fossil fuel-based energy production to environmentally sustainable methods, a strong need for safe and efficient energy storage has arisen. One well-established method is the electrochemical storage of energy in rechargeable batteries, with lithium-based batteries, in particular, having revolutionized energy storage for all sorts of electronic devices.[1,2] Lithium-based batteries alone, however, will not solve today's energy storage problems as they face a variety of challenges, ranging from limited resource availability[3] of crucial battery components over limited battery lifetimes[4] to serious safety concerns.[5] To combat the increasing resource shortages associated with lithium batteries and provide affordable and environmentally sustainable energy storage for the foreseeable future, research efforts with regards to alternative battery types have increased tremendously.[6–13] Alternatives to the current generation of lithium batteries include other alkaline batteries, replacing lithium with sodium or potassium, as well as batteries using magnesium, calcium, or aluminum.

These new battery types also suffer from various problems, ranging from a limited energy density to aging and safety concerns similar to those found in lithium-based batteries. Especially for alternative alkaline batteries employing sodium or potassium, some very similar challenges remain compared to those known for lithium batteries.[14,15] Commonly used electrolyte components like ethylene carbonate (EC), propylene carbonate (PC), dimethyl carbonate (DMC), and dimethoxyethane (DME), $LiPF_6$, $LiBF_4$, and LiTFSI, are known to be unstable in the presence of lithium-based battery anodes, leading to the formation of a passivation layer known as the solid electrolyte interphase (SEI).[16] The SEI formation poses one of the main limitations in the insufficient cycling stability of the battery, leading either to a reduced battery capacity or, in the worst case, a catastrophic thermal runaway.[10] At the same time, the SEI also acts as a protective layer preventing further electrolyte decomposition.[17]

Given this importance of the SEI, understanding the electrode/electrolyte interface has presented itself as a crucial part of improving battery performance and has been the focus of numerous studies, utilizing experimental and theoretical approaches.[18–23] One established theoretical approach for investigating the SEI formation is ab initio molecular dynamic simulation (AIMD),[18,24] which enables atomistic insights into reactions/interactions between electrolyte components and the battery anode. DFT-based AIMD simulations are generally limited by their comparatively high calculational cost, leading to short simulation times.[25] However, thanks to improving computational power, the length and time scales accessible to AIMD simulations have increased considerably so that AIMD simulations have already provided insights into the electrolyte reduction reactions and predicted decomposition pathways for the well-established lithium battery systems,[18] which were later confirmed by experimental measurements.[26] Recently

[a] D. Stottmeister, Prof. Dr. A. Groß
Institute of Theoretical Chemistry
89069 Ulm (Germany)
E-mail: daniel.stottmeister@uni-ulm.de
[b] Prof. Dr. A. Groß
Helmholtz Institute Ulm (HIU) Electrochemical Energy Storage
Helmholtzstr. 11, 89069 Ulm (Germany)
E-mail: axel.gross@uni-ulm.de

[**] A previous version of this manuscript has been deposited on a preprint server (https://doi.org/10.26434/chemrxiv-2023-6m8s1).

Supporting information for this article is available on the WWW under https://doi.org/10.1002/batt.202300156

Special Collection This publication is part of a joint Special Collection dedicated to Post-Lithium Storage, featuring contributions published in Advanced Energy Materials, Batteries & Supercaps, and ChemSusChem.

these studies have been expanded upon and applied for other battery systems like hard carbon sodium anode batteries[27] and sodium metal batteries.[28] In this paper, we have utilized DFT-based AIMD simulations to simulate various common electrolyte component interactions with lithium, sodium, and potassium surfaces. We find spontaneous dissociative adsorption events[29,30] which we carefully analyze. Note that we did not determine any reaction barriers by automatic search routines in this study. First of all, all observed reactions are more or less spontaneous and should therefore be hindered by, if at all, only rather small barriers. Second and more importantly, the reaction energetics will probably be modified by including the presence of the electrolyte whose identification will require numerically even most costly free energy calculations. Instead, here we compare the different decomposition pathways between the elements and identify similarities and differences concerning the solid electrolyte interphase formation.

Results and Discussion

Due to the dominance of lithium-based batteries, the lithium SEI is by far the most studied and consequently best understood of the alkaline metal SEIs.[31–33] The decomposition reactions of cyclic carbonates, such as ethylene carbonate (EC), propylene carbonate (PC), or vinylene carbonate (VC), in particular, have been studied extensively and have been shown to play a critical role in the formation of the SEI.[34–36] Cyclic carbonates decompose in one-electron and two-electron processes,[34] at the electrode surface,[35] allowing for a variety of decomposition products to form. The number of possible reaction products for EC alone could account for many observed electrolyte decomposition products.[36] Depending on the location of the bond cleavage, EC is expected to produce ethylene or carbon monoxide gas.[18] Both the generation of ethylene gas[37] and of CO have been found experimentally.[38] Further, AIMD simulations for the lithium metal surface have shown that the spontaneous EC decomposition occurs at a picosecond timescale.[39] First-principles electronic structure calculations have suggested a rapid decomposition of ethylene carbonate and propylene carbonate on a lithium metal surface,[40] along the reaction pathways depicted in Figure 1. When examining these reduction reactions, which were also observed on different surfaces such as LiSi,[41] one question arises: Is this purely a reduction process, or is this reaction element/site specific? In order to answer this question, a direct comparison between the decomposition reactions on Li, Na, and K was made in this study.

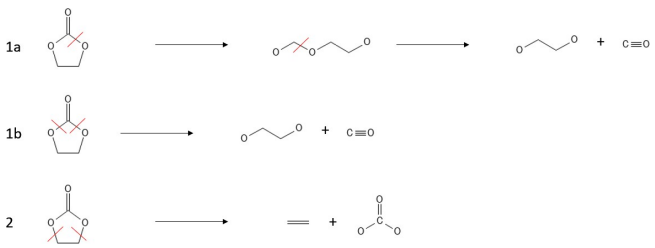

Figure 1. Observed decomposition pathways for EC on alkali metal surfaces.

We have studied the interaction of some of the most common electrolyte molecules used in alkali metal batteries, including ethylene carbonate (EC), propylene carbonate (PC) and dimethoxyethane (DME), with well-defined lithium, sodium, and potassium surfaces in order to derive chemical trends among these alkali metals. In addition, to validate our calculations we compare their results with corresponding experimental studies.[42] Further simulations for two electrolyte salts, alkali-hexafluorophosphate (MPF_6) and alkali-perchlorate ($MClO_4$) have been performed. Note that due to their still high computational demand, AIMD simulations are usually not well-suited to explore reaction mechanisms, in particular those of activated reactions. However, for several of the considered electrolyte-anode combinations, we have directly observed decomposition reactions within a simulation timeframe of 5–50 ps which means that these reactions basically occur spontaneously at the electrolyte/electrode interface. This is a first indication of the high reactivity of the alkali metal electrodes. Note furthermore, that we only considered the interaction of single molecules with the anode surfaces without really simulating the liquid nature of the electrolytes. By neglecting the interaction of the molecules with the surrounding electrolyte, we might overestimate the reactivity as the presence of solvation shells will probably weaken the molecular interaction with the metal electrode. The complex influence of the solvation behavior on the growth of the SEI in lithium metal batteries has previously been investigated.[43] Still our simulations will provide valuable insights into the electrolyte-electrode interaction as eventually the decomposition reactions at such interfaces will be dominated by the direct electrode-molecule interactions.

Simulations addressing the interaction of counter ions with alkali metal surfaces

First we address the interaction of hexafluorophosphate and perchlorate with alkali metal surfaces. Along the AIMD simulations, both perchlorate and hexafluorophosphate decomposed within a few ps. Details of the ClO_4 decomposition on Li(100) are illustrated in Figure 2. The initial physisorption step, depicted in Figure 2a, is then followed by a concerted dissociation of two oxygen atoms, resulting in the formation of ClO_2 and two oxygen atoms (Figure 2b). We further observed the dissociation into adsorbed ClO_3 and one oxygen atom (Figure 2c). Both pathways lead to the formation of Li–Cl structures at the surface while oxygen penetrates deeper into the lithium metal, creating structures that locally resemble oxide configurations (Figure 2d).[44,45] The formed Li–Cl structures loosely resemble a $Li_3Cl(100)$ surface, with the nearest neighbor distance of Cl atoms averaging at about 4 Å. We also performed AIMD runs with two additional perchlorate moities per unit cell (Figure 2c). Even for this higher perchlorate concentration, a complete separation into chloride surface and oxide subsurface structures occurred.

Research Article
doi.org/10.1002/batt.202300156
Chemistry Europe
European Chemical Societies Publishing

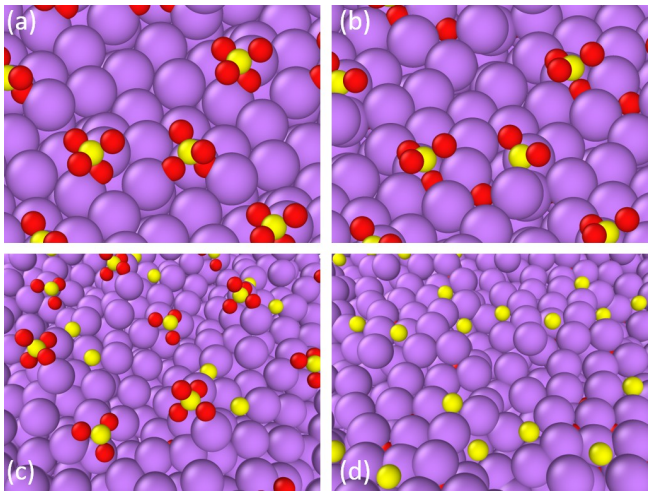

Figure 2. Snapshots of the ClO_4 decomposition simulation on Li(100). a) Initial physisorption step; b) Concerted dissociation of two oxygen atoms from one ClO_4 resulting in ClO_2 formation; c) ClO_3 adsorption after addition of two additional perchlorate moieties; d) Completed decomposition with chlorine atoms adsorbed on the surfaces and the formation of local lithium-oxide subsurface structures.

The final outcome of the AIMD runs when the lithium surface is replaced by sodium and potassium is depicted in Figure 3. On the sodium surface, we observed a similar behavior as on the lithium surface as illustrated in Figure S1 in the Supporting Information (SI). After approximately 7.5 ps, one ClO_4 ion fully decomposed in two concerted oxygen dissociation reactions. This decomposition leads to the formation of sodium oxide structures within the sodium surface, while the chloride atom remained adsorbed on the surface. While the lithium reaction occurred within less than 1.5 ps, the onset of the sodium reaction only started after 4 ps. In contrast, no reaction could be observed for the potassium surface. However, this could be a consequence of the limited simulation timeframe of the computationally demanding potassium calculations, resulting in a total runtime of under 3 ps. It is therefore likely that the simulation time was insufficient to observe the ClO_4 decomposition on potassium.

We now turn to the interaction of PF_6 with the alkaline metal anodes. Typical reaction steps of the PF_6 decomposition are illustrated in Figure 4. On the lithium surface, the PF_6 simulation started with a concerted dissociation of three fluorine atoms, resulting in the formation of LiF and PF_3

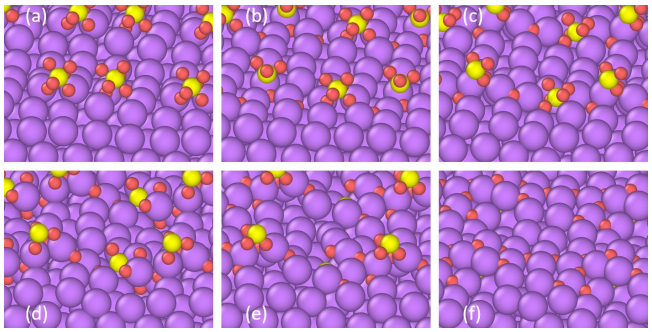

Figure 4. Reaction steps observed for the PF_6 decomposition on Li(100). a) Initial physisorption step; b) PF_3 formation; c) PF_6 surface adsorption; d) Concerted fluorine dissociation of six F; e) PF_3 adsorption; f) LiF formation.

(Figure 4b). Following this initial step, a fast reorientation of the produced PF_3 from a P-surface to an F-surface orientation occured (Figure 4c). A second concerted reaction involving three fluorine atoms followed with fluorine and phosphorous atoms sinking into the lithium surface, forming a stable Li—P—F surface. The second PF_6 molecule followed a 6-F concerted dissociation, leading to the same stable surface as the two-step reaction (Figure 4d). Similar to the ClO_4 runs, the PF_6 decomposition on the sodium surface followed the same scheme as the lithium run as illustrated in Figure S2 in the SI. While it took only three ps to fully decompose both PF_6 on the lithium surface, even after 12 ps, only one of the PF_6 molecules within the sodium run decomposed.

In contrast to the clear separation between oxide and chloride structures during the ClO_4 decomposition, no separation between fluoride and phosphate was observed upon their interaction with the Li and Na surfaces. In both cases a fluoride surface formed, with the phosphate acting as a defect within the structure. Hence we did not check the effect of higher PF_6 concentration on the resulting decomposition structures. A slightly different reaction was observed for the potassium simulation, depicted in Figure 5, where the two PF_6 molecules initially penetrated the potassium surface, sinking almost entirely into the surface and decomposing into two PF_2 moieties. Due to the limited runtime of the potassium simulations (5 ps), it is unclear whether PF_2 would further decompose or remain adsorbed on the surface.

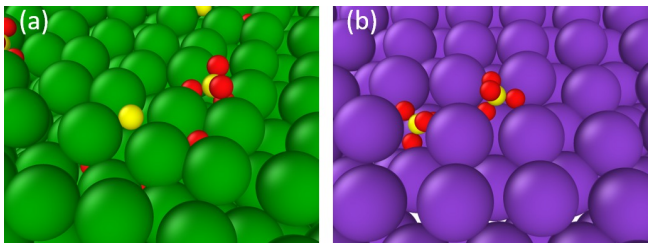

Figure 3. Final structures of the ClO_4 simulation run. a) ClO_4 on Na(100) after 15 ps; b) ClO_4 on K(100) after 3 ps.

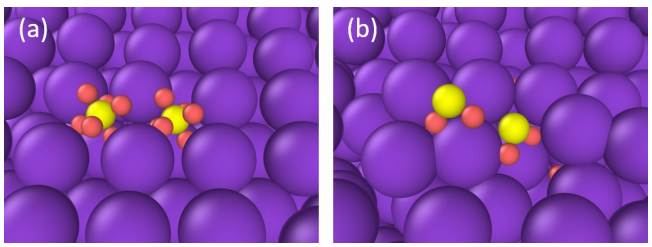

Figure 5. Snapshot of the PF_6 decomposition on K(100). a) PF_6 sinking into the K(100) surface; b) PF_2 formation.

Research Article
doi.org/10.1002/batt.202300156
Chemistry Europe
European Chemical Societies Publishing

Simulations addressing the interaction of solvent molecules with alkali metal surfaces

The cell setup for the ethylene carbonate reaction consisted of two EC molecules in a 4×4 Li(100) supercell with six Li layers. The topmost three lithium layers and the EC molecules were allowed to relax fully. The initial placement of the EC molecules has been arbitrary since the finite temperature results in sufficient molecular movement causing rather random conditions. According to the simulations, the decomposition of ethylene carbonate proceeds in two steps on the lithium metal surface, an initial ring-opening after adsorption followed by carbon monoxide formation.

Typical reaction steps of the EC decomposition are illustrated in Figure 6, where after just 30 fs of simulation time, the first EC molecule underwent decomposition via a ring-opening process (Figure 7b). In this process, the two ring oxygen atoms became coordinated by one surface lithium atom each, while the terminal oxygen penetrated the surface and assumed a two-fold coordinated position. The newly exposed carbon and oxygen atoms each form a bond with a separate surface lithium atom. This step is followed by a decarbonylation of the terminal C–O group, leaving a carbon monoxide and a de-protonated ethylene glycol molecule as reaction products (Figure 7c). This reaction is analogous to the hydrolysis of ethylene carbonate in ethylene glycol synthesis. It was also observed for propylene carbonate (PC) on lithium after 345 fs of simulation time using a similar cell setup. An alternative two-electron reaction occurred in another AIMD run in which a carbon monoxide molecule split apart from the EC molecule in a single step, resulting in the same decomposition products.

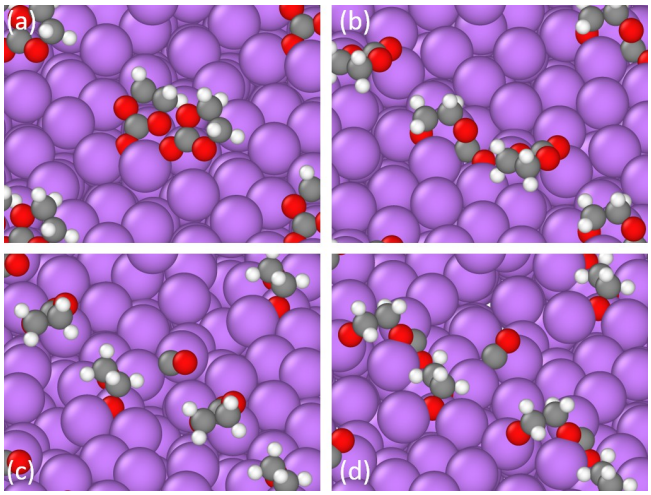

Figure 6. Reaction steps observed for the EC decomposition on Li(100). a) Initial physisorption step; b) Ring-opening of first EC molecule; c) Decarbonylation; d) Ring-opening of second EC molecule.

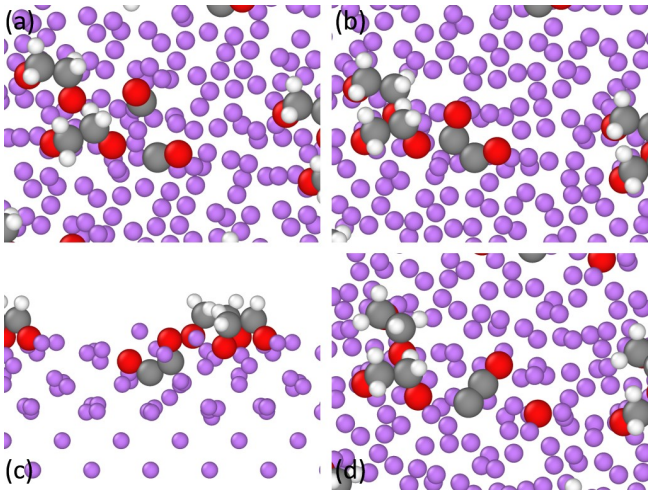

Figure 7. a) CO molecules adsorbed on Li(100) after EC decomposition, all Li atoms are scaled down; b) C–C bond formation inside Li surface; c) Side view of C–C bond formation; d) O dissociation.

Further reactions between the decomposition products occurred after the decomposition of EC on lithium. One follow-up reaction was the splitting of carbon monoxide, which resulted in the formation of carbon on the lithium surface. Such a formation of carbon on lithium metal as a consequence of CO splitting has indeed been observed via photoelectron spectroscopy.[46]

A Fischer–Tropsch process-like reaction[47] in which carbon monoxide polymerized into a carbon chain occurred on the lithium surface. While the Fisher-Tropsch process utilizes hydrogen gas to produce hydrocarbons under pressure, here, the lithium surface substitutes the hydrogen gas and allows for the formation of carbon-carbon bonds. In the first step leading to the polymerization, two EC molecules follow the CO-producing decomposition path, generating two CO molecules adsorbed on the lithium surface, see Figure 7a. The CO molecules then sink into the lithium surface, a process which has also been observed in previous studies.[48] Once both CO molecules get into proximity of one another, a C–C bond is formed, with the resulting O–C–C–O structure fully submerged in the lithium metal as depicted in Figure 7b and 7c. So far, the resulting structure is similar to ethylene glycol, with all hydrogen atoms substituted by lithium atoms. In contrast to any ethylene glycol adsorbed on the surface, the submerged structure proceeded to split off one of the two terminal oxygen atoms, changing the geometry of the molecule, resulting in an almost linear molecule with a C–C–O angle of 175°. The newly-formed C–C–O molecule remained submerged in the lithium surface for the remainder of the simulation. We suggest that this reaction can be interpreted as an initial polymerization step for the polymerization of carbon monoxide. The addition of further CO to the system could continue the reaction, forming C–C_x–O structures. While the CO polymerization on lithium metal along a Fisher-Tropsch-like process has not been reported previously, molecular lithium has previously been used to polymerize carbon monoxide.[49]

These simulation results agree with previous results, which also found both one-electron and two-electron reduction reactions.[34] No decomposition could be observed for dimethoxyethane (DME) within the simulation timeframe of 48 ps. However, the molecules strongly preferred an adsorption

Research Article
doi.org/10.1002/batt.202300156
Chemistry Europe
European Chemical Societies Publishing

configuration via an oxygen-lithium connection and remained almost stationary during the entire MD run. These findings support previous simulations, which DME observed as being "stable" on lithium metal surfaces.[50] Of course it has to be taken into account that the time scale of the AIMD simulations is much too short to really speculate about the stabilty of the adsorbed moities.

The decomposition of EC on the Na(100) surface followed the same ring-opening pathway observed on the lithium surface as illustrated in Figure S3 in the SI. No formation of carbon monoxide was observed within the 30 ps simulation time. The carbonate split-off reaction, previously found on lithium surfaces for the EC molecule,[34] was observed for PC, leading to sodium carbonate and propene gas formation, illustrated in Figure S4 in the SI. Analogous to the Li simulation, DME did not show any reactivity during the Na simulation run and preferred an O–Na–O orientation. Still, in contrast to the adsorption scenario of DME on lithium, on Na(100) the DME molecules alternated between two configurations, one being based on coordinating one sodium surface atom with both oxygen atoms, leading to a compressed molecular structure, and the other being a stretched position, where each oxygen atom coordinates a different Na surface atom. For lithium, the stretched configuration was dominant during the entire simulation run. This difference in configurational preference can be explained by the larger lattice constant of sodium, leading to longer distances between the surface metal atoms and demanding a more significant molecular deformation for the stretched orientation, when compared to lithium. Note that the observation that the decomposition reactions of EC/PC on lithium and sodium metal anodes are similar is supported by experimental IR spectroscopy, which found a very similar SEI composition for both lithium and sodium under OCV conditions.[42]

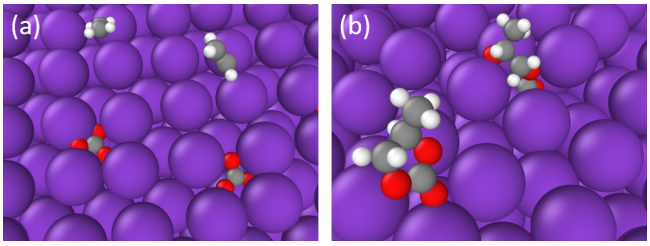

Figure 8. a) Decomposition products of two EC molecules on K(100) after 3 ps simulation time. b) Decomposition products of two PC molecules on K(100) after 3 ps simulation time.

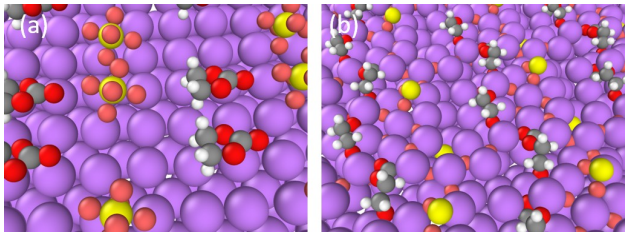

Figure 9. a) Initial setup of the EC, PF_6 mixed calculation. b) Formation of organic chains after inclusion of PF_6 in the EC decomposition simulation on a Li(100) surface.

As depicted in Figure 8, the EC/PC AIMD runs on K(100) yielded similar results as those on Na(100). No carbon monoxide formation was observed, and the molecule underwent the ring opening pathway only in the case of propylene-oxide (Figure 9b). For EC, carbonate formation under the release of ethylene gas was observed within the first 3 ps. Analogous to lithium and sodium, DME on potassium was found to be unreactive within the limited timeframe of 3 ps. Further, no clear adsorption site preference could be identified during the short simulation run. Illustrations of the DME simulations can be found in Figure S5 in the SI.

So far, all simulations only considered the interaction between the metal surface and one type of electrolyte component. In any actual cell, however, different components are mixed to form the electrolyte solution. Therefore, a cell setup containing more than one species was employed to make the simulations more realistic. For this simulation, two electrolyte solvent (EC) and two counterion (PF_6) molecules were considered per (4×4) Li(100) surface unit cell. The reactions observed in this mixed setup (see Figure 9), were the same as with the pure simulation setups, suggesting that as long as there is still an exposed lithium surface, the decomposition mechanisms are independent of each other for this specific combination. Still, while the initial reduction reaction was seemingly independent of the presence of PF_6, the change in surface composition, namely the LiF formation, led to the formation of chain-like structures, which may influence possible follow up reactions.

Up to here, the molecular dynamics simulations have indicated that, in contrast to lithium, sodium and potassium surface behave rather similarly. The decomposition of both investigated counter ions on Na(100) and K(100) showed only minor differences, with only the PF_2 formation on K being a potential difference. DME was stable throughout all simulations on all surfaces and showed only variations in its mobility, being less mobile on lithium than sodium and potassium. Both ethylene carbonate and propylene carbonate adsorption consistently resulted either in carbon monoxide or carbonate surface structure formation, with the exception that no carbon monoxide formation was observed on potassium surface. To understand whether this was just a consequence of the limited simulation timescale or a real difference, we investigated the two decomposition reactions for both PC and EC more closely. Due to the consistently small timeframes on which the observed reactions occur (< 20 ps), it seems unlikely that the observed reactions exhibit high reaction barriers. Low kinetic barriers would imply that any relevant difference between the two possible reaction paths is thermodynamic, not kinetic (the preexponential factor for a monomolecular decomposition should be dependent on the entropy of activation). We, therefore, calculated the reaction energies for the complete decomposition of both EC and PC on Li, Na, and K as follows:

$$E_{reaction} = E_{products} - E_{educt} \quad (1)$$

Research Article
doi.org/10.1002/batt.202300156
Chemistry Europe
European Chemical Societies Publishing

Table 1. Calculated reaction energies for the EC/PC decomposition pathways on Li, Na and K.

	EC, CO Path	PC, CO Path	EC, CO_3 Path	PC, CO_3 Path
Li	−3.05 eV	−4.10 eV	−4.50 eV	−4.32 eV
Na	−1.18 eV	−1.80 eV	−3.60 eV	−3.67 eV
K	+1.53 eV	+1.06 eV	−4.00 eV	−3.89 eV

Here $E_{products}$ and E_{educt} are the respective energies of the adsorbed molecules on the alkali metal surface. The calculated reaction energies are listed in Table 1, Figure 10 provides a visual representation of the decomposition thermodynamics for EC. No frequencies were calculated within the scope of this work, therefore we did not consider the influence of the zero point energy on the reaction energies.

CO_3 formation is favorable for all investigated surfaces for both EC and PC. There is, however, a substantial difference with respect to the preference of the CO_3 vs CO formation between the alkali metals. While the energetic difference between the two paths is relatively small for lithium, for sodium and potassium CO formation is energetically much more unfavorable, as illustrated in Figure 11. CO formation even becomes endothermic on potassium, thus explaining the absence of CO in the potassium simulations. Young et al. investigated the same reaction pathways for EC on a Ca surface and concluded that similar to K in our study the carbonate-producing pathway should be thermodynamically favorable for the Ca surface. They further investigated the kinetics of the two reactions, finding the carbonate reaction to be favorable from a kinetic point of view as well.[51]

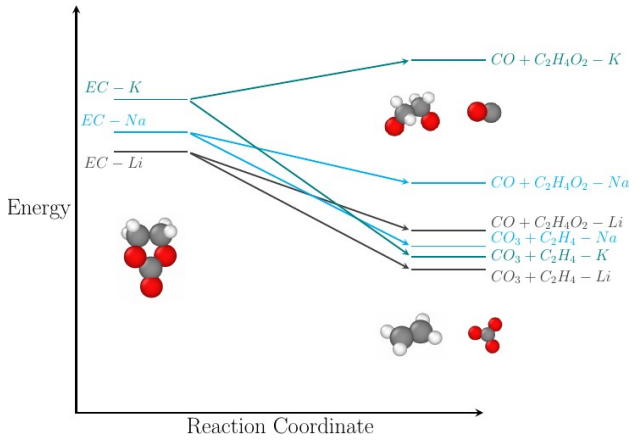

Figure 10. Visualization of the EC decomposition thermodynamics, the CO_3 producing reaction is found to be favorable for all tested metal surfaces.

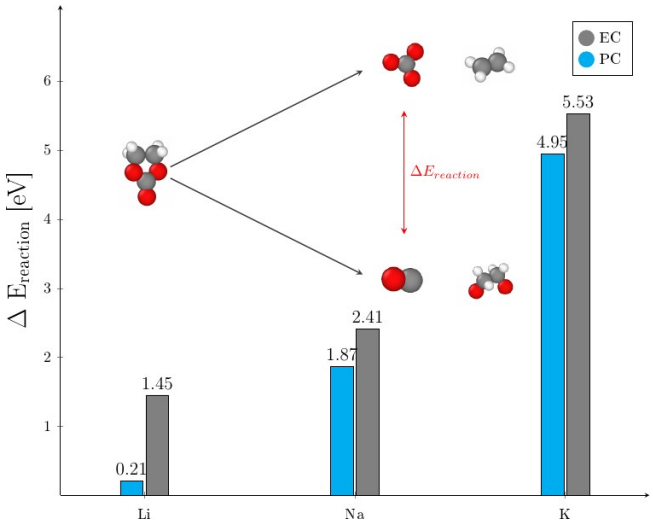

Figure 11. Comparison of the energetic preference of the CO_3 forming reaction between the tested metal surfaces.

This much more pronounced preference for the CO_3 formation on sodium and especially potassium would likely have further consequences for the formation of the solid electrolyte interphase. Within our simulations, any CO_3 formed on the metals during the decomposition reaction would lead to an MCO_3 surface structure. At the same time, the organic byproducts do not adsorb on the metal surface, but leave it instead. However, the CO decomposition paths lead to follow-up reactions withthe organic byproducts, thus leading to vastly different interface structures.

We propose that the results of this work, and others like it, while only addressing the initial steps of the SEI formation, can be used to take the next steps in advancing our understanding of the SEI in alkali metal batteries. By mapping and understanding the decomposition reactions occurring at the metal-electrolyte interface, it is possible to understand possible follow-up reactions and extrapolate the structural properties of the formed SEI. We suggest the next steps on the atomistic simulation level should focus on reactions of the initial decomposition products, forming oligomers and eventually leading to polymers. The structure of the polymers that form should be highly correlated to the composition of the decomposition products. With a solid understanding of the origins of the building blocks of these organic SEI components, we may unlock new regulating screws with which to improve the battery performance. Following the same logic, one can take a close look at the influence of common additives like Vinylcarbonate (VC) or Fluoro ethylene carbonate (FEC) on the formation of polymeric SEI components. Finally, we propose to take a closer look at the influence of the evolving surfaces on the possible follow-up reactions. As this work has shown, chloride-rich and carbonate-rich surfaces are formed directly from the electrolyte decomposition. However, these surfaces will not interact with the remaining decomposition products in the same way as the respective metal surface, likely enabling new reactions while restricting others.

Research Article
doi.org/10.1002/batt.202300156

Conclusion

Performing ab initio molecular dynamics simulations, we have compared the initial decomposition reactions of common electrolyte components on lithium, sodium, and potassium surfaces. At room temperature, the reactions occurred almost spontaneously within picoseconds on all investigated surfaces. While the decomposition of electrolyte salts did not exhibit any significant differences between lithium and sodium, leading to metal-oxide and metal-halide structures, the formation of PF_2 was observed on the potassium surface. We further found a clear separation between an oxygen-rich surface structure and a chloride surface layer for the decomposition of perchlorate on sodium and lithium. DMC was found to be non-reactive within the simulation timeframe. The initial cyclic carbonate decomposition results in two sets of products, yielding either carbon monoxide or leading to carbonate formation. The carbonate-forming reaction was found to be energetically favorable on all considered alkali metal surfaces, though the difference in reaction energies between the two reactions increased from less than 1 eV for PC on lithium to over 5 eV for EC on potassium. This indicates a strong selectivity towards the formation of K_2CO_3 in the case of the potassium surfaces. The selectivity of initial decomposition reactions is expected to strongly influence the formation of the solid electrolyte interphase since the formation of organic compounds was not observed in the carbonate reaction. In contrast, multiple secondary reactions involving carbon monoxide were observed, including the formation of C–C bonds along a Fischer–Tropsch process-like mechanism. While sodium and potassium overall were found to behave rather similarly to lithium in most situations, we were still able to identify key differences in the initial decomposition processes. Understanding and controlling these initial decomposition reactions and their products – the building blocks of the SEI – might be a pathway to stabilize the SEI in post-lithium batteries.

Experimental

The electrolyte decomposition reactions have been modeled using first-principles density functional theory (DFT) calculations within the plane-wave-based Vienna ab initio simulation package (VASP)[52] framework. To better account for chemisorption, the exchange-correlation was calculated using the revised Perdew–Burke–Ernzerhof functional (RPBE).[53] The electron-core interactions were described via the projector augmented wave (PAW) method.[54,55] The alkali anode surfaces were modeled using a 6-layer slab with a 4×4 geometry and a vacuum region of >20 Å, using the (100) surface termination. A Γ centered 5×5×1 k-point grid was used to calculate the energies. Total energies were converged up to 10^{-5} eV using the Methfessel-Paxton smearing scheme[56] with a width of 0.2 eV, with the ionic geometry being converged to energetic differences below 10^{-4} eV. Note that all calculations were performed for charge-neutral systems. Although we also consider the interaction of ions with the metal surfaces, upon adsorption these ions become coupled to the electron reservoir of the metal anodes, so that it is more appropriate to consider the adsorbate system as being overall charge-neutral.

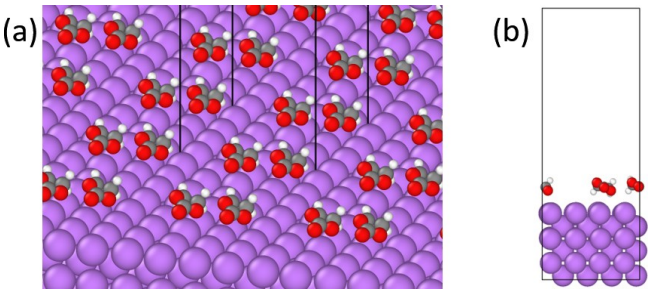

Figure 12. a) View of the simulation cell used for the AIMD simulation of EC on Li(100). b) Side view of the MD simulation cell for the EC decomposition.

To include dispersion effects, the DFT-D3 vdW correction of Grimme[57] was applied. The molecular dynamics simulations have been performed within a canonical ensemble using the Nose thermostat with a Nose-frequency of 10^{14} Hz at a temperature of 300 K. A typical cell setup for the MD simulations is shown in Figure 12. The simulations included between 2–6 electrolyte molecules explicitly, further electrolyte molecules were neither explicitly nor implicitly considered, which is a simplification since, in an actual cell, there is no vacuum following the first electrolyte molecules but rather a solution of various components. The absence of solvent molecules means that the performed simulations cannot catch any solvation effects and might overestimate the interactions between the electrolyte molecules and the surface. There is, however, one advantage of neglecting of solvation effects since, without any attractive interaction between different electrolyte layers, the adsorbed molecules are expected to be more reactive concerning the surface. This increased reactivity is beneficial because of the limited simulation timeframe of just a few picoseconds, which otherwise would make any observation of surface reactions very costly.

Acknowledgements

This work contributes to the research performed at CELEST (Center for Electrochemical Energy Storage Ulm-Karlsruhe) and was funded by the Deutsche Forschungsgemeinschaft (DFG, German Research Foundation) under Germany's Excellence Strategy – EXC 2154 – Project number 390874152. The authors furthermore acknowledge computer time supplied by the state of Baden-Württemberg through the bwHPC project and the Germany Research Foundation (DFG) through grant number INST 40/467-1 FUGG (JUSTUS cluster). Open Access funding enabled and organized by Projekt DEAL.

Conflict of Interest

The Authors declare no Conflict of Interest.

Data Availability Statement

The data that support the findings of this study are available from the corresponding author upon reasonable request.

Keywords: Density Functional Theory · Na-Batteries · K-Batteries · Solid-Electrolyte Interphase · Ab initio Molecular Dynamics Simulations

[1] N. Björn, N. Måns, *Nat. Clim. Change* **2015**, *5*, 329.
[2] M. Ishikawa, M. Kanemoto, M. Morita, *J. Power Sources* **1999**, *81–82*, 217.
[3] G. Martin, L. Rentsch, M. Höck, M. Bertau, *Energy Storage Mater.* **2017**, *6*, 171 .
[4] J. P. Pender, G. Jha, D. H. Youn, J. M. Ziegler, I. Andoni, E. J. Choi, A. Heller, B. S. Dunn, P. S. Weiss, R. M. Penner, C. B. Mullins, *ACS Nano* **2020**, *14*, 1243.
[5] Y. Chen, Y. Luo, H. Zhang, C. Qu, H. Zhang, X. Li, *Small Methods* **2019**, *3*, 1800551.
[6] A. D. Khudyshkina, P. A. Morozova, A. J. Butzelaar, M. Hoffmann, M. Wilhelm, P. Theato, S. S. Fedotov, F. Jeschull, *ACS Appl. Polym. Mater.* **2022**, *4*, 2734.
[7] I. Hasa, P. Adelhelm, G. Cao, L. Mai, *Batteries & Supercaps* **2021**, *4*, 1036.
[8] M. Walter, M. V. Kovalenko, K. V. Kravchyk, *New J. Chem.* **2020**, *44*, 1677.
[9] S. Lv, J. Yuan, Z. Chen, P. Gao, H. Shu, X. Yang, E. Liu, S. Tan, M. Ruben, Z. Zhao-Karger, M. Fichtner, *ChemSusChem* **2020**, *13*, 2286.
[10] M. Jäckle, K. Helmbrecht, M. Smits, D. Stottmeister, A. Groß, *Energy Environ. Sci.* **2018**, *11*, 3400.
[11] K. Pfeifer, M. F. Greenstein, D. Aurbach, X. Luo, H. Ehrenberg, S. Dsoke, *ChemElectroChem* **2020**, *7*, 3487.
[12] H. Euchner, B. P. Vinayan, M. A. Reddy, M. Fichtner, A. Groß, *J. Mater. Chem. A* **2020**, *8*, 14205.
[13] Y. Ma, Y. Ma, H. Euchner, X. Liu, H. Zhang, B. Qin, D. Geiger, J. Biskupek, A. Carlsson, U. Kaiser, A. Groß, S. Indris, S. Passerini, D. Bresser, *ACS Energy Lett.* **2021**, *6*, 915.
[14] M. Sawicki, L. L. Shaw, *RSC Adv.* **2015**, *5*, 53129.
[15] R. Rajagopalan, Y. Tang, X. Ji, C. Jia, H. Wang, *Adv. Funct. Mater.* **2020**, *30*, 1909486.
[16] M. Zachman, S. Choudhury, L. Archer, L. Kourkoutis, *Nature* **2018**, *560*, 345.
[17] J. Han, H. Euchner, M. Kuenzel, S. M. Hosseini, A. Groß, A. Varzi, S. Passerini, *ACS Energy Lett.* **2021**, *6*, 3063.
[18] K. Leung, J. L. Budzien, *Phys. Chem. Chem. Phys.* **2010**, *12*, 6583.
[19] W. Aiping, K. Sanket, L. Hong, Q. Yue, *npj Comp. Mater.* **2018**, *4*.
[20] K. Forster-Tonigold, J. Kim, J. Bansmann, A. Groß, F. Buchner, *ChemPhysChem* **2021**, *22*, 441.
[21] B. Li, Y. Chao, M. Li, Y. Xiao, R. Li, K. Yang, X. Cui, G. Xu, L. Li, C. Yang, Y. Yu, D. P. Wilkinson, J. Zhang, *Electrochem. Energy Rev.* **2023**, *6*, 7.
[22] H. Wang, D. Zhai, F. Kang, *Energy Environ. Sci.* **2020**, *13*, 4583.
[23] J. Popovic, *J. Electrochem. Soc.* **2022**, *169*, 030510.
[24] H. Euchner, A. Groß, *Phys. Rev. Mater.* **2022**, *6*, 040302.
[25] A. Groß, S. Sakong, *Chem. Rev.* **2022**, *122*, 10746.
[26] T. Li, P. B. Balbuena, *Chem. Phys. Lett.* **2000**, *317*, 421.
[27] F. A. Soto, A. Marzouk, F. El-Mellouhi, P. B. Balbuena, *Chem. Mater.* **2018**, *30*, 3315.
[28] X. Chen, X. Shen, B. Li, H.-J. Peng, X.-B. Cheng, B.-Q. Li, X.-Q. Zhang, J.-Q. Huang, Q. Zhang, *Angew. Chem. Int. Ed.* **2018**, *57*, 734.
[29] A. Groß, M. Scheffler, *Chem. Phys. Lett.* **1996**, *256*, 417.
[30] A. Groß, A. Eichler, J. Hafner, M. J. Mehl, D. A. Papaconstantopoulos, *Surf. Sci.* **2003**, *539*, L542.
[31] X.-B. Cheng, R. Zhang, C.-Z. Zhao, Q. Zhang, *Chem. Rev.* **2017**, *117*, 10403.
[32] B. Horstmann, F. Single, A. Latz, *Curr. Opin. Electrochem.* **2019**, *13*, 61.
[33] X. He, D. Bresser, S. Passerini, F. Baakes, U. Krewer, J. Lopez, C. T. Mallia, Y. Shao-Horn, I. Cekic-Laskovic, S. Wiemers-Meyer, F. A. Soto, V. Ponce, J. M. Seminario, P. B. Balbuena, H. Jia, W. Xu, Y. Xu, C. Wang, B. Horstmann, R. Amine, C.-C. Su, J. Shi, K. Amine, M. Winter, A. Latz, R. Kostecki, *Nat. Rev. Mater.* **2021**, *6*, 1036.
[34] Y. Wang, S. Nakamura, M. Ue, P. B. Balbuena, *J. Am. Chem. Soc.* **2001**, *123*, 11708.
[35] N. I. Hammer, R. J. Hinde, R. N. Compton, K. Diri, K. D. Jordan, D. Radisic, S. T. Stokes, K. H. Bowen, *J. Chem. Phys.* **2004**, *120*, 685.
[36] Y. Jin, N.-J. H. Kneusels, P. C. M. M. Magusin, G. Kim, E. Castillo-Martínez, L. E. Marbella, R. N. Kerber, D. J. Howe, S. Paul, T. Liu, C. P. Grey, *J. Am. Chem. Soc.* **2017**, *139*, 14992–15004.
[37] C. L. Campion, W. Li, B. L. Lucht, *J. Electrochem. Soc.* **2005**, *152*, A2327.
[38] M. Onuki, S. Kinoshita, Y. Sakata, M. Yanagidate, Y. Otake, M. Ue, M. Deguchi, *J. Electrochem. Soc.* **2008**, *155*, A794.
[39] J. Yu, P. B. Balbuena, J. Budzien, K. Leung, *J. Electrochem. Soc.* **2011**, *158*, A400.
[40] M. Ebadi, D. Brandell, C. M. Araujo, *J. Chem. Phys.* **2016**, *145*, 204701.
[41] K. Hankins, F. A. Soto, P. B. Balbuena, *J. Electrochem. Soc.* **2017**, *164*, E3457.
[42] D. I. Iermakova, R. Dugas, M. R. Palacín, A. Ponrouch, *J. Electrochem. Soc.* **2015**, *162*, A7060.
[43] Y. Xiao, X. Wang, K. Yang, J. Wu, Y. Chao, C. Xi, M. Li, Q. Zhang, Z. Liu, L. Li, Y. Yu, C. Yang, *Energy Storage Mater.* **2023**, *55*, 773.
[44] J. Rogal, K. Reuter, M. Scheffler, *Phys. Rev. B* **2007**, *75*, 205433.
[45] B. R. Didar, L. Yashina, A. Groß, *ACS Appl. Mater. Interfaces* **2021**, *13*, 24984.
[46] G. Zhuang, Y. Chen, P. N. Ross, *Surf. Sci.* **1998**, *418*, 139.
[47] A. de Klerk, *Fischer–Tropsch Process*, pages 1–20, American Cancer Society **2013**.
[48] L. E. Camacho-Forero, T. W. Smith, S. Bertolini, P. B. Balbuena, *J. Phys. Chem. C* **2015**, *119*, 26828.
[49] B. Wang, G. Luo, M. Nishiura, Y. Luo, Z. Hou, *J. Am. Chem. Soc.* **2017**, *139*, 16967.
[50] L. E. Camacho-Forero, T. W. Smith, S. Bertolini, P. B. Balbuena, *J. Phys. Chem. C* **2015**, *119*, 26828.
[51] J. Young, M. Smeu, *J. Phys. Chem. Lett.* **2018**, *9*, 3295.
[52] G. Kresse, J. Furthmüller, *Phys. Rev. B* **1996**, *54*, 11169.
[53] B. Hammer, L. B. Hansen, J. K. Nørskov, *Phys. Rev. B* **1999**, *59*, 7413.
[54] P. E. Blöchl, *Phys. Rev. B* **1994**, *50*, 17953.
[55] G. Kresse, D. Joubert, *Phys. Rev. B* **1999**, *59*, 1758.
[56] M. Methfessel, A. T. Paxton, *Phys. Rev. B* **1989**, *40*, 3616.
[57] S. Grimme, J. Antony, S. Ehrlich, H. Krieg, *J. Chem. Phys.* **2010**, *132*, 154104.

Manuscript received: April 13, 2023
Revised manuscript received: May 22, 2023
Accepted manuscript online: May 24, 2023
Version of record online: June 21, 2023